Proceedings of the 10th Brazilian Congress of Thermal Sciences and Engineering – ENCIT 2004
Braz. Soc. of Mechanical Sciences and Engineering – ABCM, Rio de Janeiro, Brazil, Nov. 29 – Dec. 03, 2004

Paper CIT04-0077

SECONDARY INSTABILITY OF VARICOSE MODE IN GÖRTLER FLOW

Leandro F. de Souza
USP - Universidade de São Paulo
Instituto de Ciências Matemáticas e de Computação – Departamento de Ciências de Computação e Estatística
Av. Trabalhador São Carlense, 400 - SP - 13560-970, Brazil
lefraso@icmc.usp.br

Márcio T. Mendonça
Centro Técnico Aeroespacial, Instituto de Aeronáutica e Espaço
Pç Mal. Eduardo Gomes, 50 - São José dos Campos, SP - 12228 904, Brazil
marcio_tm@yahoo.com

Marcello A. Faraco de Medeiros
USP - Universidade de São Paulo
Escola de Engenharia de São Carlos - Departamento de Engenharia Aeronáutica
Av. Trabalhador São Carlense, 400 - SP - 13566-590, Brazil
marcello@sc.usp.br

Abstract. *The growth of Görtler vortices in boundary layers over concave surfaces is responsible for a strong distortion of the velocity profiles in the normal and spanwise directions. The resulting inflectional velocity profiles are subject to secondary instability which may result in the development of horseshoe vortices. This type of secondary instability is known as the varicose mode. In the present study the varicose mode is investigated using direct numerical simulation. The governing equations based on the vorticity-velocity formulation are solved using compact finite differences in the normal and longitudinal directions. In the spanwise direction the flow is assumed periodic. A Runge-Kutta time marching scheme was used to integrate in time. The differences between the present results and the results for secondary stability from other authors are discussed.*

keywords: *Görtler Vortices, Secondary stability, Hydrodynamic instability, Laminar flow transition, horseshoe vortices.*

1. Introduction

The centrifugal instability mechanism for boundary layers over concave surfaces is responsible for the development of counter-rotating vortices, aligned in the streamwise direction, known as Görtler vortices (Görtler, 1940). These vortices develop mushroom type structures resulting in strongly inflectional streamwise velocity profiles both in the normal and spanwise directions. These velocity profiles are unstable to others disturbances and secondary instability may set in either as a sinuose or a varicose mode as found experimentally by Swearingen and Blackwelder, 1987.

Hall and Horseman, 1991 analyzed the secondary stability characteristics of Görtler vortices. They present the eigenfunctions of the streamwise u and wall normal velocity component v of the most unstable modes. In Fig. 1 their streamwise eigenfunction u for the varicose mode is shown. This eigenfunction was obtained by the secondary stability analysis of a velocity profile corresponding to $\overline{x} = 100$ cm of the Swearingen and Blackwelder, 1987 experiment. They considered a spanwise wavelength $\overline{\lambda} = 2,3$ cm, which corresponds to the wavelength of one particular vortex pair found by Swearingen and Blackwelder, 1987. Their eigenfunction for the wall normal velocity component v is shown in Fig. 2. An amplitude peak was found for u at the top of the mushroom structure centered with respect to the upwash region. Two smaller amplitude peaks were found on each side of the mushroom.

Yu and Liu, 1991 and Yu and Liu, 1994 studied the linear stability of the distorted streamwise profile caused by the Görtler flow. The experiment of Swearingen and Blackwelder, 1987 was again used as reference. Their analysis corresponds to the streamwise position $\overline{x} = 90$ cm of the experiment. They assumed that the spanwise wavelength was $\overline{\lambda} = 1,8$ cm. This value corresponds to the mean spanwise wavelength observed in the experiments. Both sinuose and varicose modes were analyzed. Yu and Liu, 1994 show the most unstable

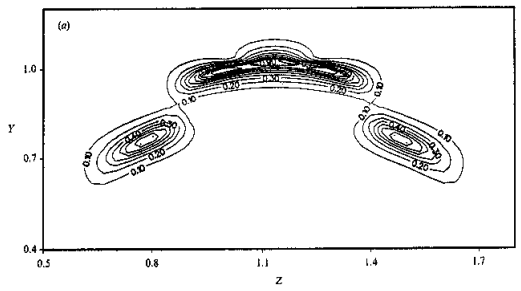

Figure 1: Autofunction u of the secondary instability of the varicose mode (Hall and Horseman, 1991).

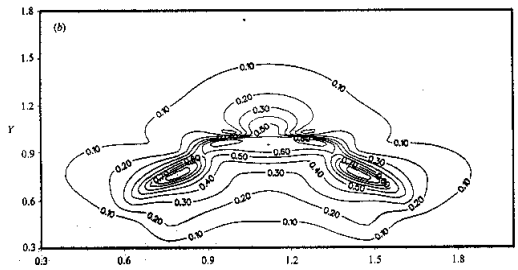

Figure 2: Autofunction v of the secondary instability of the varicose mode (Hall and Horseman, 1991).

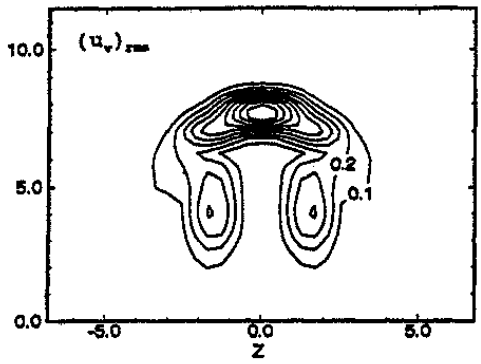

Figure 3: Secondary instability Autofunction u for the varicose mode (Yu and Liu, 1994).

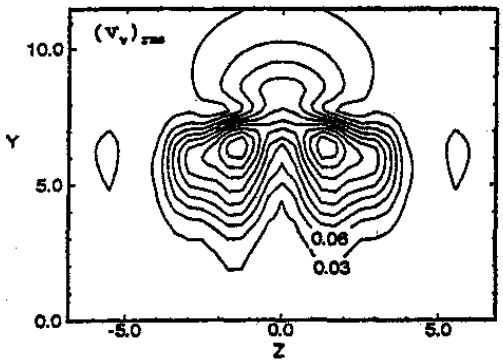

Figure 4: Secondary instability Autofunction v for the varicose mode (Yu and Liu, 1994).

eigenfunctions for the u, v and w component velocities. Those results for the varicose mode are shown in the Figs. 3, 4 and 5. The results are in qualitative agreement with the results obtained by Hall and Horseman, 1991 regarding the location of the velocity peaks with respect to the mushroom structure.

Li and Malik, 1995 also used the experiment of Swearingen and Blackwelder, 1987 to analise the stability of the Görtler flow. They performed an inviscid secondary stability analysis for the profile found at $x^* = 95$ cm. Their most unstable varicose mode eigenfunction u is shown in Fig. 6. The second most unstable varicose mode eigenfunction u was also obtained and is shown in Fig. 7. The streamwise isovelocity lines are also shown. One can observe that the position of the eigenfunction u is strongly related to the inflection point in the velocity profile.

In the present work the secondary stability of the Görtler flow is analyzed by means of spatial direct numerical simulation. High frequency disturbances were introduced in a flow that was destabilized first by centrifugal stability, causing the birth of Görtler vortices. The flow parameters adopted for this investigation are the same used in the experiment of Swearingen and Blackwelder, 1987. Only secondary instability of the varicose type will be considered, allowing a reduction in the computational cost due to the symmetries present in the resulting solution vectors with respect to the spanwise direction.

2. Formulation

In this study, the governing equations are the incompressible, unsteady Navier-Stokes equations with constant density and viscosity. They consist of the momentum equations for the velocity components (u, v, w) in the streamwise direction (x), wall normal direction (y) and spanwise direction (z):

$$\frac{\partial u}{\partial t} + u\frac{\partial u}{\partial x} + v\frac{\partial u}{\partial y} + w\frac{\partial u}{\partial z} = -\frac{\partial p}{\partial x} + \nabla^2 u, \tag{1}$$

$$\frac{\partial v}{\partial t} + u\frac{\partial v}{\partial x} + v\frac{\partial v}{\partial y} + w\frac{\partial v}{\partial z} + \frac{Go^2(u^2)}{\sqrt{Reh}} = -\frac{\partial p}{\partial y} + \nabla^2 v, \tag{2}$$

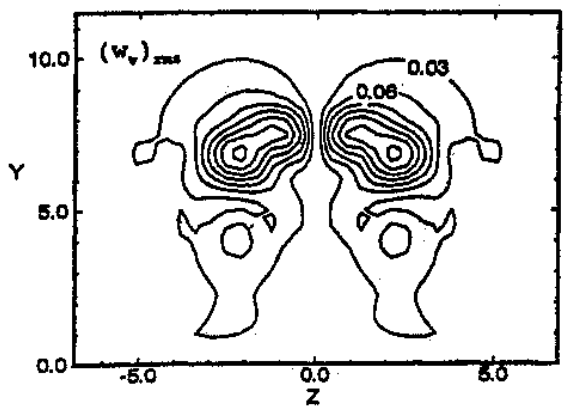

Figure 5: Secondary instability Autofunction w for the varicose mode Yu and Liu, 1994.

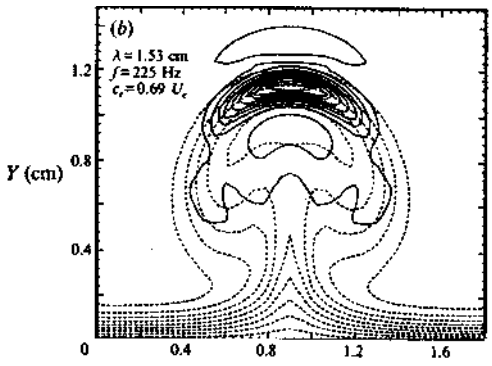

Figure 6: secondary instability Autofunction u for the most unstable varicose mode Li and Malik, 1995.

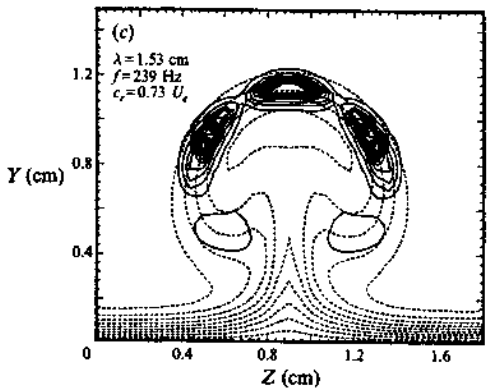

Figure 7: secondary instability Autofunction u for the second most unstable varicose mode Li and Malik, 1995.

$$\frac{\partial w}{\partial t} + u\frac{\partial w}{\partial x} + v\frac{\partial w}{\partial y} + w\frac{\partial w}{\partial z} = -\frac{\partial p}{\partial z} + \nabla^2 w, \tag{3}$$

and the continuity equation:

$$\frac{\partial u}{\partial x} + \frac{\partial v}{\partial y} + \frac{\partial w}{\partial z} = 0, \tag{4}$$

where p is the pressure and $\nabla^2 = \frac{1}{Re}\left(\frac{\partial^2}{\partial x^2} + \frac{\partial^2}{\partial y^2} + \frac{\partial^2}{\partial z^2}\right)$.

The variables used in the above equations are non-dimensional. They are related to the dimensional variables by:

$$x = \frac{\overline{x}}{\overline{L}}, \quad y = \frac{\overline{y}}{\overline{L}}, \quad z = \frac{\overline{z}}{\overline{L}}, \quad k_c = \frac{\overline{L}}{\overline{R}}, \quad u = \frac{\overline{u}}{\overline{U}_\infty}, \quad v = \frac{\overline{v}}{\overline{U}_\infty}, \quad w = \frac{\overline{w}}{\overline{U}_\infty}, \quad t = \overline{t}\frac{\overline{U}_\infty}{\overline{L}}, \quad Re = \frac{\overline{U}_\infty \overline{L}}{\overline{\nu}},$$

where Re is the Reynolds number, the terms with an overline are dimensional terms, $\overline{L}$ is the reference length, $\overline{U}_\infty$ is the free-stream velocity, $\overline{\nu}$ is the kinematic viscosity and $\overline{R}$ is the radius of curvature.

The Görtler number is given by $Go = (\overline{k}_c\sqrt{Re})^{1/2}$. In these equations, the term $(Go^2u^2)/(\sqrt{Re}h)$ is the leading order curvature term, where $h = 1 - \overline{k}_c y$ and $\overline{k}_c$ is the curvature of the wall.

The vorticity is defined as the negative curl of velocity vector. Taking the negative curl of the momentum equations (1) to (3) and using the fact that both the velocity and the vorticity fields are solenoidal, one can obtain the vorticity transport equation in each direction:

$$\frac{\partial \omega_x}{\partial t} + \frac{\partial a}{\partial y} - \frac{\partial b}{\partial z} + \frac{Go^2}{\sqrt{Re}h}\frac{\partial (u^2)}{\partial z} = \nabla^2 \omega_x, \tag{5}$$

$$\frac{\partial \omega_y}{\partial t} + \frac{\partial c}{\partial z} - \frac{\partial a}{\partial x} = \nabla^2 \omega_y, \tag{6}$$

$$\frac{\partial \omega_z}{\partial t} + \frac{\partial b}{\partial x} - \frac{\partial c}{\partial y} - \frac{Go^2}{\sqrt{Re}h}\frac{\partial (u^2)}{\partial x} = \nabla^2 \omega_z, \tag{7}$$

where $a = v\omega_x - u\omega_y$, $b = u\omega_z - w\omega_x$ and $c = w\omega_y - v\omega_z$ are the nonlinear terms resulting from convection, vortex stretching and vortex bending.

Taking the definition of the vorticity and the mass conservation equation, one can obtain a Poisson equation for each velocity component:

$$\frac{\partial^2 u}{\partial x^2} + \frac{\partial^2 u}{\partial z^2} = -\frac{\partial \omega_y}{\partial z} - \frac{\partial^2 v}{\partial x \partial y}, \tag{8}$$

$$\frac{\partial^2 v}{\partial x^2} + \frac{\partial^2 v}{\partial y^2} + \frac{\partial^2 v}{\partial z^2} = -\frac{\partial \omega_z}{\partial x} + \frac{\partial \omega_x}{\partial z}, \tag{9}$$

$$\frac{\partial^2 w}{\partial x^2} + \frac{\partial^2 w}{\partial z^2} = \frac{\partial \omega_y}{\partial x} - \frac{\partial^2 v}{\partial y \partial z}. \tag{10}$$

The flow is assumed to be periodic and symmetric with respect to $z = 0$ in the spanwise (z) direction. Therefore, the flow field is expanded in real Fourier cosine and sine series with K spanwise Fourier modes:

$$(u, v, \omega_z, b, c) = \sum_{k=0}^{K} (U_k, V_k, \Omega_{z_k}, B_k, C_k)\cos(\beta_k z), \quad (w, \omega_x, \omega_y, a) = \sum_{k=1}^{K} (W_k, \Omega_{x_k}, \Omega_{y_k}, A_k)\sin(\beta_k z). \tag{11}$$

where β_k is the spanwise wavenumber given by $\beta_k = 2\pi k/\lambda_z$, and λ_z is the spanwise wavelength of the fundamental spanwise Fourier mode.

Substituting the cosine and sine transforms (Eq. 11) in the vorticity transport equations (5 to 7) and in the velocity Poisson equations (8 to 10) yields the governing equations in the Fourier space:

$$\frac{\partial \Omega_{x_k}}{\partial t} + \frac{\partial A_k}{\partial y} - \beta_k B_k - \frac{Go^2}{\sqrt{Re}}\frac{\beta_k (U_k^2)}{h} = \nabla_k^2 \Omega_x, \tag{12}$$

$$\frac{\partial \Omega_{y_k}}{\partial t} + \beta_k C_k - \frac{\partial A_k}{\partial x} = \nabla_k^2 \Omega_y, \tag{13}$$

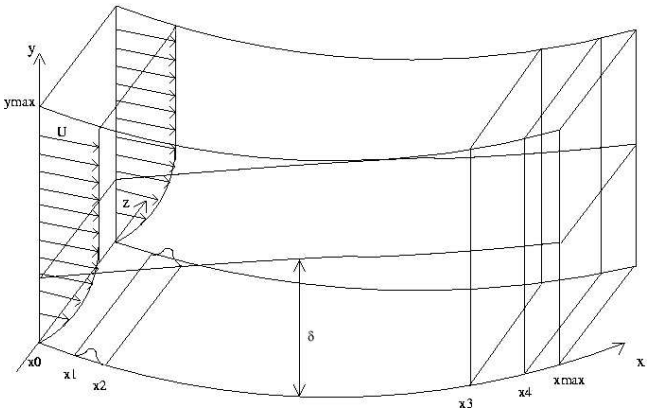

Figure 8: Integration domain.

$$\frac{\partial \Omega_{z_k}}{\partial t} + \frac{\partial B_k}{\partial x} + \frac{\partial C_k}{\partial y} - \frac{Go^2}{\sqrt{Re}h}\frac{\partial (U_k^2)}{\partial x} = \nabla_k^2 \Omega_z, \tag{14}$$

$$\frac{\partial^2 U_k}{\partial x^2} - \beta_k^2 U_k = -\beta_k \Omega_{y_k} - \frac{\partial^2 V_k}{\partial x \partial y}, \tag{15}$$

$$\frac{\partial^2 V_k}{\partial x^2} + \frac{\partial^2 V_k}{\partial y^2} - \beta_k^2 V_k = -\frac{\partial \Omega_{z_k}}{\partial x} + \beta_k \Omega_{x_k}, \tag{16}$$

$$\frac{\partial^2 W_k}{\partial x^2} - \beta_k^2 W_k = \frac{\partial \Omega_{y_k}}{\partial x} + \beta_k \frac{\partial V_k}{\partial y}, \tag{17}$$

where $\nabla_k^2 = \frac{1}{Re}\left(\frac{\partial^2}{\partial x^2} + \frac{\partial^2}{\partial y^2} - \beta_k^2\right)$.

The governing equations are complemented by the specification of boundary conditions. At the wall no-slip and no penetration conditions are imposed, except at the suction and blowing region where the wall-normal velocity component is specified. At the inflow the velocity and vorticity components are specified based on the Blasius boundary layer solution. At the upper boundary the vorticity disturbances decay exponentially to zero. Finally, at the outflow boundary the second derivative of all dependent variables are set to zero.

3. Numerical Method

The Eqs.(12) to (17) are solved numerically inside the integration domain shown schematically in Fig. 8. The calculation are done on an orthogonal uniform grid, parallel to the wall. The fluid enters the computational domain at $x = x_0$ and exits at the outflow boundary $x = x_{max}$. Disturbances are introduced into the flow field using a suction and blowing function at the wall in a disturbance strip. This region is located between x_1 and x_2. In the region located between x_3 and x_4 a buffer domain technique was implemented in order to avoid wave reflections at the outflow boundary. In these simulations a Blasius boundary layer is used as the base flow.

At the inflow boundary ($x = x_0$), all velocity and vorticity components are specified. At the outflow boundary ($x = x_{max}$), the second derivative of the velocity and vorticity components in the streamwise direction are set to zero. At the upper boundary ($y = y_{max}$) the flow is assumed to be irrotational. This is satisfied by setting all vorticity and their derivatives to zero. An exponential decay of the velocity is imposed using the condition:

$$\frac{\partial V_k}{\partial y}|_{x,y_{max},t} = -\frac{\beta_k}{\sqrt{Re}} V_k(x, y_{max}, t). \tag{18}$$

At the wall ($y = 0$), no-slip conditions are imposed for the streamwise (U_k) and the spanwise (W_k) velocity components. For the wall-normal velocity component (V_k) the non-permeability and no-penetration conditions are imposed in all points at the wall except between x_1 and x_2, where the disturbances are introduced. In addition, the condition $\partial V_k/\partial y = 0$ is imposed to ensure conservation of mass. The equations used for evaluating the vorticity components at the wall are:

$$\frac{\partial^2 \Omega_{x_k}}{\partial x^2} - \beta_k^2 \Omega_{x_k} = -\frac{\partial^2 \Omega_{y_k}}{\partial x \partial y} - \beta_k \nabla_k^2 V_k \quad \text{and} \quad \frac{\partial \Omega_{z_k}}{\partial x} = \beta_k \Omega_{x_k} - \nabla_k^2 V_k. \tag{19}$$

The introduction of the disturbances at the wall is done via a slot in the region ($i_1 \leq i \leq i_2$), where i_1 and i_2 are, respectively, the first and the last point of the disturbance strip, in the x direction. The function used for the variation of the normal velocity V_k along the streamwise direction is:

$$V_k(i,0,t) = A\sin^3(\epsilon) \quad \text{for} \quad i_1 \leq i \leq i_2 \quad \text{and} \quad V_k(x,0,t) = 0 \quad \text{for} \quad i < i_1 \quad \text{and} \quad i > i_2, \tag{20}$$

where $\epsilon = \pi(i - i_1)/(i_2 - i_1)$ and A is a real constant that can be chosen to adjust the amplitude of the disturbance. The variable i indicates the grid point location x_i in the streamwise direction, and points i_1 and i_2 correspond to x_1 and x_2 respectively.

A damping zone near the outflow boundary is defined in which all the disturbances are gradually damped down to zero. This technique is use to avoid reflections in the outflow boundary. Meitz and Fasel, 2000, adopted a fifth order polynomial, and the same function is used in the present model. The basic idea is to multiply the vorticity components by a ramp function $f_2(x)$ after each step of the integration method. Using this technique, the vorticity components are taken as:

$$\Omega_k(x,y) = f_2(x)\Omega_k(x,y,t), \tag{21}$$

where $\Omega_k(x,y,t)$ is the disturbance vorticity component that comes out from the Runge-Kutta integration and $f_2(x)$ is a ramp function that goes smoothly from 1 to 0. The implemented function was:

$$f_2(x) = f(\epsilon) = 1 - 6\epsilon^5 + 15\epsilon^4 - 10\epsilon^3, \tag{22}$$

where $\epsilon = (i - i_3)/(i_4 - i_3)$ for $i_3 \leq i \leq i_4$. The points i_3 and i_4 correspond to the positions x_3 and x_4 in the streamwise direction respectively. To ensure good numerical results a minimum distance between x_3 and x_4 and between x_4 and the end of the domain - x_{max} should be specified. The zones in the simulations presented here has 30 grid points in each region.

Another buffer domain, located near the inflow boundary is also implemented in the code. As pointed out by Meitz, 1996, in simulations involving streamwise vortices, reflections due to the vortices at the inflow can contaminate the numerical solution. The dumping function is similar to the one used for the outflow boundary:

$$f_3(x) = f(\epsilon) = 6\epsilon^5 - 15\epsilon^4 + 10\epsilon^3, \tag{23}$$

where ϵ is $\epsilon = (i - 1)/(i1 - 1)$ for the range $1 \leq i \leq i_1$. All the vorticity components are multiplied by this function in this region.

The time derivatives in the vorticity transport equations were discretized with a classical 4^{th} order Runge-Kutta integration scheme (Ferziger and Peric, 1997). The spatial derivatives were calculated using a 6^{th} order compact finite difference scheme (Souza et al., 2002a; Souza et al., 2002b). The V-Poisson equation (16) was solved using a Full Approximation Scheme (FAS) multigrid (Stüben and Trottenberg, 1981). A v-cycle working with 4 grids was implemented.

4. Numerical Results

In the current numerical study the parameters were identical to those used in the experiment of Swearingen and Blackwelder, 1987. They considered the stability of a boundary layer over a concave plate with constant radius $\overline{R} = 3,2$ m and constant free stream velocity $\overline{U}_\infty = 5$ m/s. The Reynolds number based on the characteristic length $\overline{L} = 10$ cm was $Re = 33124$. The Görtler number at the inlet boundary was $Go = 2,389$ and the dimensional wavelength was $\overline{\lambda} = 1.8$ cm, which corresponds to $\beta = 34,9$. Along the streamwise and wall normal directions 441 and 321 grid points were used respectively. In the spanwise direction 11 Fourier modes were used. In the experiment a non stationary disturbance of 130 Hz was observed, and a disturbance with this frequency was introduced in the present numerical simulation.

Figures 9 to 11 present the root mean square (rms) of the non stationary disturbance velocity components in the streamwise, normal and spanwise directions at the streamwise position $x = 11.02$. In this figures the mean streamwise velocity profile due to the Görtler vortices is also shown by dashed contour lines, varying from 0.1 to 0.9. In Fig. 9 the largest value of the u_{rms} of about 3.6% is located at the central region ($z = 0$). This u_{rms} peak is located above the wall where the mean flow streamwise velocity is $0.7\overline{U}_\infty$. This is the location of the inflection point in the streamwise mean velocity component. This result are in qualitative agreement with the results obtained by Hall and Horseman, 1991; Yu and Liu, 1994 and Li and Malik, 1995 for the first varicose mode, with a single dominant peak at the head of the mushroom. The weaker peaks close to the wall as shown in Fig. 9 are not captured by an inviscid analysis and are associated to viscous effects (Li and Malik, 1995).

The normal and spanwise disturbance velocity components have more complex structures with stronger v_{rms} peaks located above and inside the mushroom. The w_{rms} has strong peaks on either sides of the mushroom. Figure 10 presents the isolines of v_{rms}. The results are in qualitative agreement with Hall and Horseman, 1991

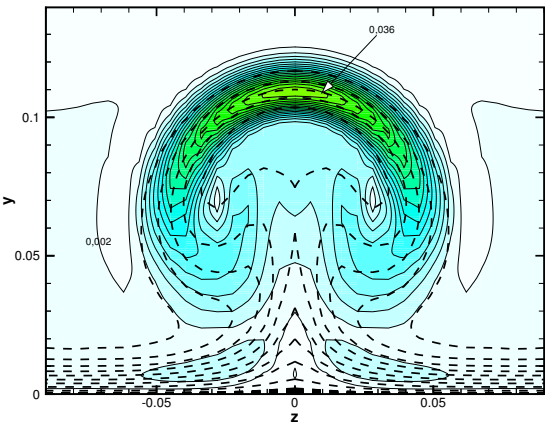

Figure 9: Contour: u_{rms}. Dashed: GV.

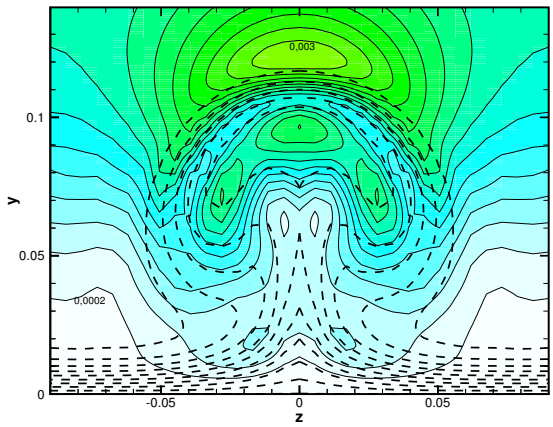

Figure 10: Contour: v_{rms}. Dashed: GV.

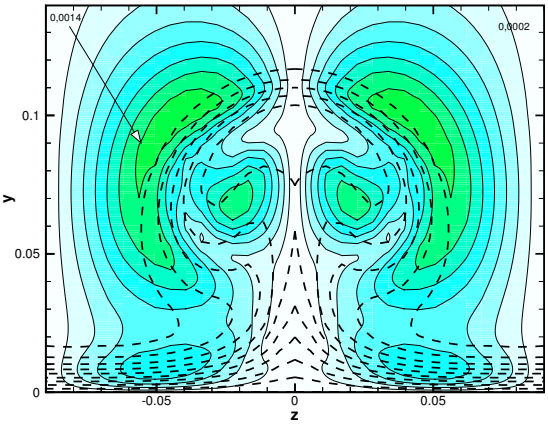

Figure 11: Contour: w_{rms}. Dashed: GV.

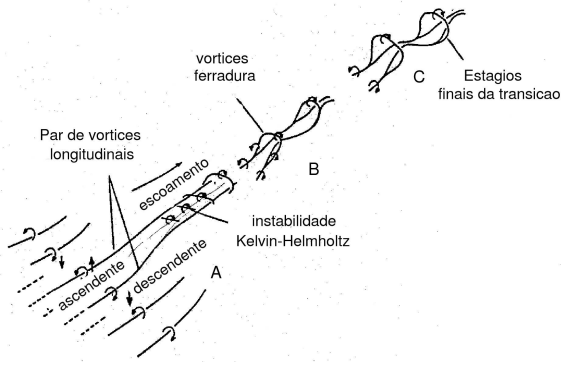

Figure 12: Schematic representation of the formation of horseshoe type vortices from Görtler vortices (Floryan, 1991).

and Yu and Liu, 1994, with a velocity peak at the center. But in the present study the largest amplitudes of the v_{rms} occurred above the mushroom structure. This difference may be because Hall and Horseman, 1991 and Yu and Liu, 1994 considered a parallel mean flow for the secondary stability analysis, discarding the normal and spanwise velocity components of the mushroom.

The results for w_{rm} shown in Fig. 11 are also in qualitative agreement with the analysis of Yu and Liu, 1994. In the present results the two peaks on either side of the mushroom head are farther apart from each other when compared to the results from Yu and Liu, 1994. These peaks are located at the outer layer of the mushroom, while in Yu and Liu, 1994 they are located inside the mushroom structure. Again, this discrepancy with Yu and Liu, 1994 may be attributed to the parallel assumption used in that work.

Görtler vortices secondary instabilities have growth rates much stronger than the vortices itself, which leads the flow to breakdown to a turbulent regime very fast. This fast growth justify the use of parallel flow approximation. Nevertheless, for Görtler vortices, the spanwise plane is the one where the nonlinear effects are stronger and the normal and spanwise velocity components may have a strong contribution to the development of the secondary instability.

The development of the horseshoe type structure observed in the varicose mode was described by Floryan, 1991. In the upwash region, due to the resulting inflectional velocity profile, a Kelvin-Helmholtz inviscid instability develops. Therefore, spanwise vorticity located at the head of the mushroom structure is generated. This vorticity connect the counter-rotating longitudinal vortices and lift up, forming the head of the horseshoe. A schematic representation of this process is shown in Fig. 12. The velocity field presented in Figs. 10 and 11 are well correlated to the structures associated with the mechanism described above.

The streamwise evolution of the secondary instability eigenfunction is presented in Fig. 13 to 15. Iso-contours of the root mean square secondary instability streamwise velocity component for three different streamwise positions ($x = 9.46, 10$ and $10, 48$) are presented. The growth of the mushroom structure and the corresponding growth of the secondary instability eigenfunction are shown. As the longitudinal vortices grow in intensity and height, the strength of the secondary instability also grows. The u_{rms} peak located at the center ($z = 0$) is

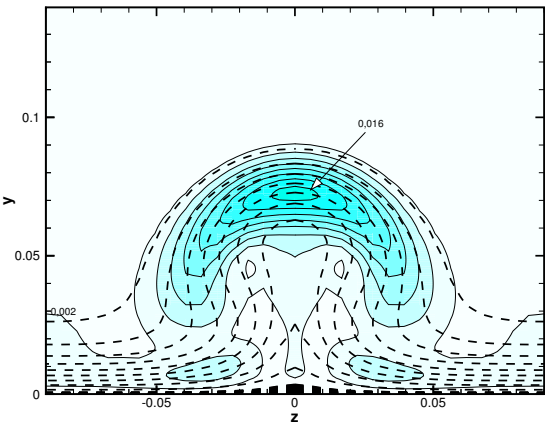

Figure 13: Iso-velocity contours of u_{rms}. $x = 9,46$.

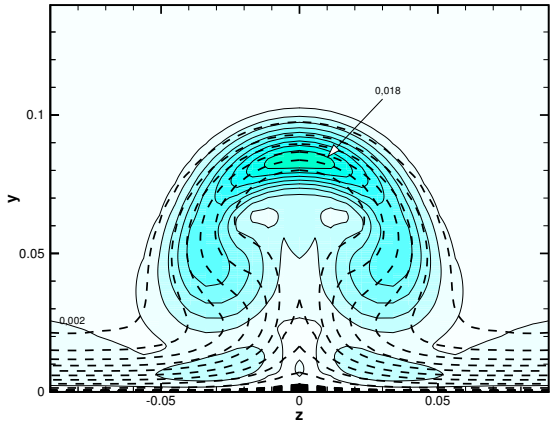

Figure 14: Iso-velocity contours u_{rms}. $x = 10,00$.

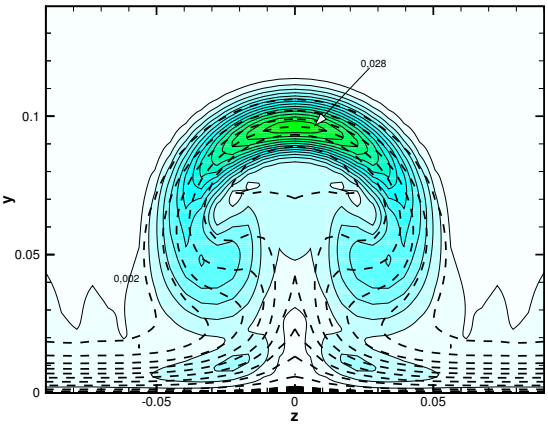

Figure 15: Iso-velocity contours u_{rms}. $x = 10,48$.

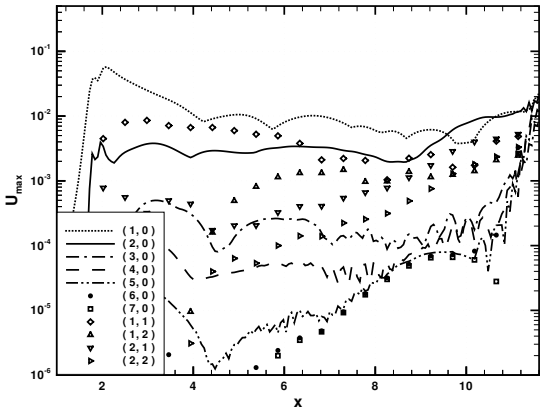

Figure 16: Autofunction u amplitude variation in the streamwise direction. Unsteady Fourier modes.

lifted by the mushroom and follows the position of the mean velocity profile inflectional point.

Figure 16 shows the streamwise amplitude variation of different Fourier modes. Only the time dependent modes are shown. This modes are a consequence of the unsteady disturbance introduced at the suction and blowing strip. Initially this unsteady modes are stable, but as the mushroom structure develops and promote inflectional velocity profiles around $x = 10$, they grow as secondary instability to the new distorted mean flow. This secondary instability evolves very rapidly in the streamwise direction leading the flow to a initial turbulent state.

In Figs. 17 and 18 Q isosurfaces are shown for a given time t. The Q isosurfaces are obtained by the method described in Dubief and Delvayre, 2000 and represent the vortical structure of the flow. The streamwise extent covers a region from earlier nonlinear Görtler vortex up to the secondary instability region. These structures agree with the structures observed experimentally (Swearingen and Blackwelder, 1987) and with the proposed mechanism described by Floryan, 1991 and presented in Fig. 12.

5. Conclusions

In this work the secondary stability of Görtler vortices to non stationary disturbances were analyzed. The results were in good agreement with results from previous investigations. The mushroom structures observed in the experiment of Swearingen and Blackwelder, 1987 were recovered in the numerical simulation. The direct numerical simulation model was able to take into account nonlinear, nonparallel and viscous effects which result in small differences from previous investigations. By relaxing the symmetry hypothesis in the spanwise direction, the sinuose mode of secondary instability will be investigated in a future work, along with the effect of the Görtler vortices spanwise wavenumber.

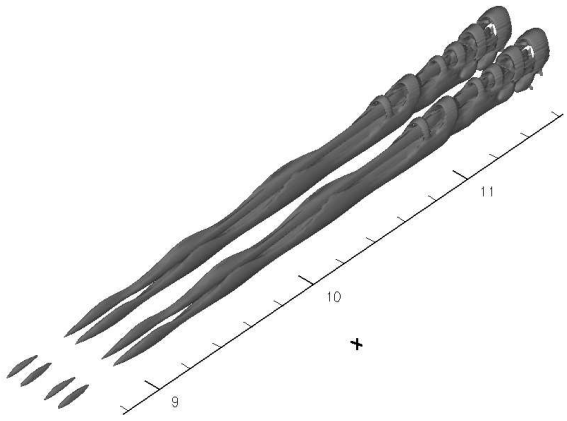

Figure 17: The horseshoe structure, perspective.

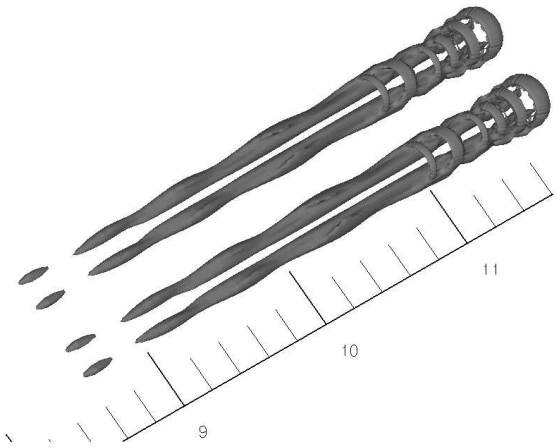

Figure 18: The horseshoe structure, top view.

6. Acknowledgments

The financial support from FAPESP (State of Sao Paulo Research Support Foundation) – Grant numbers 00/04943-7 and 03/05027-2 – is greatly acknowledged.

7. References

Dubief, Y. and Delvayre, F., 2000, On coherent-Vortex Identification in Turbulence, "J. of Turbulence", Vol. **011**, pp. 1–22.

Ferziger, J. H. and Peric, M., 1997, "Computational Methods for Fluid Dynamics", Springer-Verlag Berlin Heidelberg New York.

Floryan, J. M., 1991, On the Görtler Instability of Boundary Layers, "Prog. Aerospace Sci.", Vol. **28**, pp. 235–271.

Görtler, H., 1940, On the three-dimensional instability of laminar boundary layers on concave walls, Technical Report NACA TM-1375, National Advisory Commitee for Aeronautics – NACA.

Hall, P. and Horseman, N. J., 1991, The Linear Inviscid Secondary Instability of Longitudinal Vortex Structures in Boundary Layers, "J. Fluid Mech.", Vol. **232**, pp. 357–375.

Li, F. and Malik, M. R., 1995, Fundamental and Subharmonic Secondary Instability of Görtler Vortices, "J. Fluid Mech.", Vol. **297**, pp. 77–100.

Meitz, H. L., 1996, "Numerical Investigation of Suction in a Trasitional Flat-Plate Boundary Layer", PhD thesis, The University of Arizona.

Meitz, H. L. and Fasel, H. F., 2000, A compact-difference scheme for the Navier-Stokes equations in vorticity-velocity formulation., "J. Comp. Phys.", Vol. **157**, pp. 371–403.

Souza, L. F., Mendonça, M. T., and de Medeiros, M. A. F., 2002a, Assessment of different numerical schemes and grid refinement for hydrodynamic stability simulations, "9th brazilian congress on thermal engineering and sciences", Caxambu - MG.

Souza, L. F., Mendonça, M. T., de Medeiros, M. A. F., and Kloker, M., 2002b, Analisys of Tollmien-Schlichting waves propagation on a flat plate with a Navier-Stokes solver, "9th brazilian congress on thermal engineering and sciences", Caxambu - MG.

Stüben, K. and Trottenberg, U., 1981, "Nonlinear multigrid methods, the full approximation scheme", chapter 5, pp. 58–71, Lecture Notes in Mathematics. Köln-Porz.

Swearingen, J. D. and Blackwelder, R. F., 1987, The Growth and Breakdown of Streamwise Vortices in the Presence of a Wall, "J. Fluid Mech.", Vol. **182**, pp. 255–290.

Yu, X. and Liu, J. T. C., 1991, The secondary Instability in Goertler Flow, "Physics of Fluids", Vol. **A3**, pp. 1845–1847.

Yu, X. and Liu, J. T. C., 1994, On the Mechanism of Sinuos and Varicose Modes in Three-Dimensional Viscous Secondary Instability of Nonlinear Görtler rolls, "Physics of Fluids", Vol. **6**, pp. 736–750.